LANGMUIR

Article

pubs.acs.org/Langmuir

# Synergistic Growth of Giant Wormlike Micelles in Ternary Mixed Surfactant Solutions: Effect of Octanoic Acid

Gergana S. Georgieva,[†] Svetoslav E. Anachkov,[†] Ingo Lieberwirth,[‡] Kaloian Koynov,[‡] and Peter A. Kralchevsky*[,†]

[†]Department of Chemical and Pharmaceutical Engineering, Faculty of Chemistry and Pharmacy, Sofia University, 1 James Bourchier Blvd., 1164 Sofia, Bulgaria

[‡]Max Planck Institute for Polymer Research, 10 Ackermannweg, 55128 Mainz, Germany

Supporting Information

**ABSTRACT:** The synergistic growth of giant wormlike micelles in ternary mixed solutions composed of an anionic surfactant (sodium laurylethersulfate, SLES), a zwitterionic surfactant (cocamidopropyl betaine, CAPB), and octanoic acid (HC8) is studied. Rheological data and their analysis in terms of Cole−Cole plots and micellar characteristic times are presented, and the micellar structures behind the observed rheological behavior are revealed by cryo-TEM micrographs. The surfactant composition is fixed near the maximal micelle size of the binary SLES + CAPB system, whereas the concentration of HC8 is varied. At a given HC8 concentration, the viscosity of the ternary micellar solutions exhibits a very high and sharp peak. Polarized-light optical microscopy indicates that all investigated solutions are isotropic rather than liquid-crystalline. The cryo-TEM imaging shows complex phase behavior: wormlike micelles to the left of the peak, giant entangled wormlike micelles at the peak, and long wormlike micelles coexisting with multiconnected micellar aggregates to the right of the peak. The formation of multiconnected micelles leads to a drop in viscosity at the higher concentrations. The results contribute to a better understanding of the structure−rheology relations in micellar surfactant solutions and could be useful for controlling the properties of formulations in personal-care and house-hold detergency.

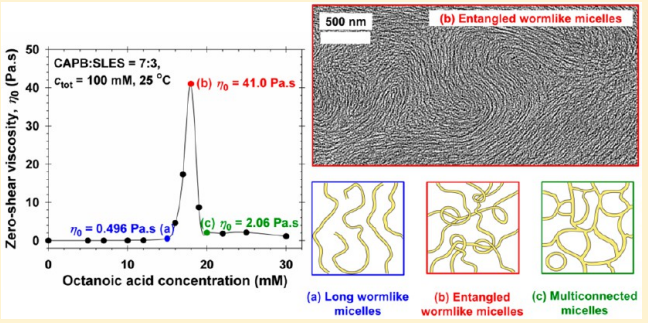


## 1. INTRODUCTION

Slightly above the critical micelle concentration (CMC), surfactants form spherical micelles, and the viscosity of their solutions is close to that of water. However, in the presence of electrolytes or cosurfactants, amphiphilic molecules can assemble into wormlike micelles or living polymers.[1] Above a certain micellar volume fraction, the worms intertwine and form a transient micellar network, which gives rise to viscoelastic behavior. With respect to the fundamental aspect, the relationship between the structure and rheology of concentrated micellar solutions has attracted considerable attention.[2−13] In the applied aspect, formulations containing wormlike micelles are frequently used as thickeners in cosmetics and home care[14−16] and even as drug-delivery vehicles in biomedicine.[15]

In numerous studies on concentrated micellar solutions, one could find many different ways to form wormlike micelles. Among them, the most common worm-forming systems consist of (i) an ionic surfactant and a salt or hydrotrope;[2−4,13,17−26] (ii) an ionic surfactant with nonionic and/or zwitterionic additives;[27−35] (iii) two oppositely charged surfactants;[36−41] (iv) nonionic, gemini, or biological surfactants;[42−48] and (v) a surfactant and a cosurfactant.[49−53] An extensive list of formulations containing wormlike micelles can be found in ref 15.

Many worm-forming surfactant solutions show complex phase behavior and nonmonotonic trends in their viscoelastic properties. Rehage and Hoffmann[2,3] were among the first to demonstrate that the addition of salts or hydrotropes to cationic surfactant solutions induces micellar growth, and the zero-shear viscosity passes through one or even two peaks as a function of the concentration of additive. Similar nonmonotonic rheological behavior was later observed in many other surfactant systems.[4,13,18−24,29−35,38−40,42,44−46] The viscosity typically increases because of a transition from spherical to elongated and then to wormlike micelles. With the increase in surfactant concentration, the wormlike micelles intertwine and form a transient network, which leads to a considerable rise in viscosity.

However, in many systems the viscosity decreases at higher concentrations of the additive, which is counterintuitive. A summary of the different pathways explaining the viscosity reduction was first presented in ref 40 and was further expanded in ref 54. Three of the possible mechanisms are (1)

**Received:** November 1, 2016
**Published:** November 14, 2016





DOI: 10.1021/acs.langmuir.6b03955
*Langmuir* 2016, 32, 12885−12893

micellar branching, which is the formation of dynamic connections between micelles that can either slide along the micelle or form 4-fold ghostlike crossings;[11,12,55,56] (2) micellar shortening, in which the micelles diminish in size at higher concentrations of the additive, which is especially common in catanionic mixtures,[14,22,40] and (3) shape or phase transition, in which worms transform into discs or isotropic micellar solutions are converted into liquid-crystalline mesophases.[57] To reveal the mechanism of viscosity reduction in a given system, direct cryo-TEM imaging should be applied.

Our goal in the present article is to examine the rheology–structure relations for ternary mixed micellar solutions, which contain a zwitterionic surfactant (cocamidopropyl betaine, CAPB), an anionic surfactant (sodium laurylethersulfate, SLES), and a nonionic cosurfactant (octanoic acid, HC8). From both a fundamental and applied viewpoint, such systems are interesting because they exhibit a high and sharp peak in viscosity as a function of fatty acid concentration, which could be applied to control the rheological properties of shampoo-like formulations. To reveal the relationships between the complex rheological behavior and the microstructural evolution, we employed cryogenic TEM.

The paper is organized as follows. In Section 2, we give a brief overview of the theory used in the subsequent analysis of the rheological results. Section 3 provides information about the materials and experimental methods used. In Section 4, the experimental results are presented and discussed. Special attention is paid to the relation between microstructure and rheology.

## 2. THEORETICAL BACKGROUND

The rheological properties of wormlike micelles (or living polymers) in the semidilute regime are often described by Cates' model.[5−9] In this model, the stress relaxation mechanisms include (i) reptation (moving like a snake in long grass), which denotes the curvilinear diffusion of a wormlike micelle between the neighboring micelles,[58] and (ii) reversible scission,which is the ability of the micelles to break and recombine. The overall rheological response is governed by the ratio $\zeta = \tau_{break}/\tau_{rep}$ of the characteristic breaking time $\tau_{break}$ to the characteristic time for reptation $\tau_{rep}$. Provided that $\tau_{break} \ll \tau_{rep}$, i.e., $\zeta \ll 1$, such wormlike micellar solutions behave as Maxwellian fluids with a single relaxation time $\tau_R$ given by[5,6]

$$\tau_R \cong (\tau_{break}\tau_{rep})^{1/2} \tag{1}$$

Under oscillatory shear, the storage $G'$ and loss $G''$ moduli for a Maxwellian viscoelastic body obey the relationships[59]

$$G' = \frac{\omega^2\tau_R^{\,2}}{1+\omega^2\tau_R^{\,2}}G_0, \quad G'' = \frac{\omega\tau_R}{1+\omega^2\tau_R^{\,2}}G_0 \tag{2}$$

where $\omega$ is the angular frequency of oscillations and $G_0$ is the high-frequency plateau value of the elastic modulus. In the Maxwell model, the absolute value of the complex viscosity $|\eta^*|$ is given by the expression[59]

$$|\eta^*| = \frac{G_0\tau_R}{\sqrt{1+\omega^2\tau_R^{\,2}}} \tag{3}$$

Let $\omega_c$ be the crossover frequency at which $G' = G''$. The latter equality, along with eq 2, implies that $\omega_c\tau_R = 1$, hence $\tau_R = 1/\omega_c$ and $G_0 = 2G'$ at the crossover point. Having determined both $G_0$ and $\tau_R$, one can calculate the zero-frequency viscosity $\eta_{\omega=0}$ as well as the correlation length $\xi$:[2,3,6,59]

$$\eta_{\omega=0} = G_0\tau_R, \quad \xi \approx \left(\frac{k_BT}{G_0}\right)^{1/3} \tag{4}$$

The expression for $\eta_{\omega=0}$ follows from eq 3; $\xi$ characterizes the mesh size of the transient micellar network. Using eq 2, one can check that $G'$ and $G''$ satisfy the equation

$$(G' - G_{osc})^2 + G''^2 = G_{ocs}^{\,2} \tag{5}$$

where $G_{osc} = G_0/2$. This is an equation of circumference in the plane $(G',G'')$, which can be used to verify the validity of the Maxwell model by constructing a Cole–Cole plot ($G''$ vs $G'$).[8,9,17,59] For wormlike micellar solutions, however, deviations from the pure Maxwellian behavior typically occur at high frequencies and result in an upturn in the viscous modulus $G''$.[8,9,17] These phenomena can be explained as a transition in the relaxation mode from reptation to breathing or Rouse modes. To quantify the departure from the pure Maxwell model, Turner and Cates[8] introduced the parameter

$$\bar{\zeta} = \frac{\tau_{break}}{\tau_R} \tag{6}$$

which can be determined by comparing numerical and experimental Cole–Cole plots (see below). Using eq 6 and the obtained $\bar{\zeta}$, one can estimate $\tau_{break}$ from purely viscoelastic data.

## 3. MATERIALS AND METHODS

**3.1. Materials.** In the present study, we investigate the growth of giant micelles in ternary surfactant solutions. We studied a mixture of two surfactants and a cosurfactant (fatty acid), which are as follows: (i) a zwitterionic surfactant–cocamidopropyl betaine (CAPB), $M$ = 342.52 g/mol, product of Goldschmidt GmbH, Germany with commercial name TEGO Betain F50 and (ii) an anionic surfactant, sodium laurylethersulfate, with one ethylene-oxide group (SLES-1EO or briefly SLES), $M$ = 332.43 g/mol, product of Stepan Co., USA, with commercial name STEOL CS-170 UB; and (iii) octanoic (caprylic) acid (HC8), $M$ = 144.21 g/mol, a product of Sigma-Aldrich, Germany. The structural formulas of the surfactants are given in Figure 1. From the product specification data of TEGO Betain F50, one sees that 100 mM CAPB contains from 81 to 120 mM NaCl. To determine the exact amount of NaCl in our batch, we performed electrolytic conductivity measurements (Appendix A and Figure S1) and found that 100 mM CAPB contains 118 ± 6 mM NaCl as an admixture.

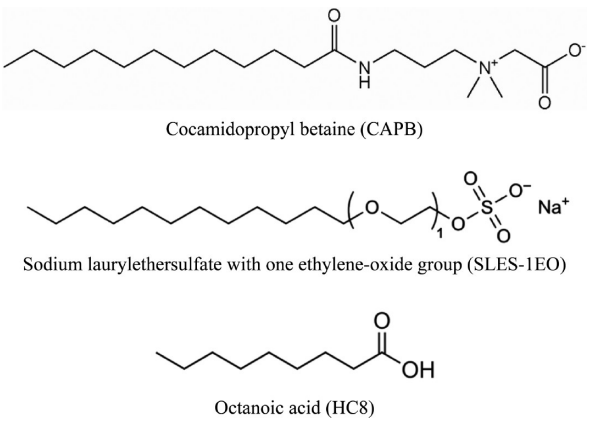


**Figure 1.** Structural formulas of the amphiphilic molecules used.



DOI: 10.1021/acs.langmuir.6b03955
Langmuir 2016, 32, 12885−12893

All chemicals were used as received without further purification. The aqueous solutions were prepared with deionized water from an Elix 3 water purification system (Merck Millipore, Merck KGaA, Germany).

**3.2. Experimental Section.** The effect of HC8 on micellar growth was studied at a fixed CAPB/SLES molar ratio equal to 7:3. The stock (binary) surfactant solution (CAPB/SLES = 7:3) was prepared in a reaction bottle and was homogenized on a magnetic stirrer at room temperature. Then, the dissolution of octanoic acid (HC8) into the mixed (binary) micelles was carried out at 70−75 °C by vigorous agitation on a temperature-controlled magnetic stirrer for at least 1.5 h. The resulting ternary micellar solution was kept in a thermostat at 25 °C for 24 h so that chemical equilibrium could be reached. After that, the solutions were used for pH and rheological measurements as well as for optical microscopy and cryo-TEM imaging.

**3.3. Rheological Measurements.** The rheological properties of the micellar solutions were characterized by a rotational rheometer (Bohlin Gemini, Malvern Instuments, U.K.) using cone-and-plate geometry with the plate temperature ($T$ = 25 °C) controlled by a Peltier unit. A solvent trap was used to minimize the change in sample composition by evaporation during each measurement. For samples with zero-shear viscosity $\eta_0$ up to ca. 40 Pa·s, we used a cone with a diameter of 60 mm and a cone angle of 2° (the gap distance is 70 $\mu$m), whereas for samples with $\eta_0$ > 40 Pa·s, we switched to a cone with a diameter of 40 mm and a cone angle of 4° (the gap distance is 150 $\mu$m). Two types of rheological experiments were carried out: (i) steady shear and (ii) stress-controlled frequency sweep.

In the regime of steady shear, the shear stress $\sigma$ was measured as a function of the shear rate $\dot{\gamma}$ in the range from 0.01 to 10 $s^{-1}$. The apparent viscosity $\eta$ and the zero-shear viscosity $\eta_0$ are defined as follows:

$$\eta(\dot{\gamma}) = \frac{\sigma}{\dot{\gamma}}, \quad \eta_0 = \lim_{\dot{\gamma}\to 0} \frac{\sigma}{\dot{\gamma}} \tag{7}$$

In the regime of stress-controlled frequency sweep (oscillatory deformation), the storage and loss moduli, $G'$ and $G''$, were measured as functions of the oscillation frequency, $\nu = \omega/(2\pi)$, in the range from 0.01 to 10 Hz at a 2% amplitude of shear deformation that was in the range of the linear viscoelastic response of the studied samples.

**3.4. Polarized-Light Optical Microscopy.** This method was used to investigate the phase behavior of the surfactant solutions. To distinguish between isotropic (micellar) and birefringent (liquid-crystalline) media, we used an Axioplan (Zeiss, Germany) optical microscope in transmitted-light polarization mode. The microscope was equipped with a polarizer, an analyzer, and a compensator (retarder). In our case, the compensator was a first-order retardation plate ($\lambda$-plate or red-I plate) positioned below the analyzer to improve visibility by introducing vivid interference colors. Birefringent specimens appeared iridescent with features that vary depending on the overall shape and molecular order.[60] Under the same conditions, isotropic (micellar) solutions were magenta-red in color without any distinguishable features.

**3.5. Cryo-TEM Imaging.** Specimens were prepared with a Vitrobot preparation unit (FEI Co., USA) at 25 °C and 100% relative humidity. A drop of solution was placed on a holey carbon TEM grid, and the excess liquid was blotted off with filter paper. The exact amount of blotting (repetitions and duration) was adjusted so as to obtain films ranging in thickness between 100 and 250 nm.[61] The blotted samples were kept in the Vitrobot for several seconds to relax from any shearing effects caused by the blotting procedure.[61] The relaxed samples were then plunged into liquid ethane (−183 °C) to form vitrified specimens that were stored in liquid nitrogen (−196 °C) until further inspection. Specimens were examined with a Tecnai F20 transmission electron microscope (FEI Co., USA) with an integrated electron energy-loss spectrometer. The microscope operated at an acceleration voltage of 200 kV using a Gatan cryo-specimen holder that maintained the vitrified specimens below −175 °C. To minimize the electron-beam radiation damage, we used the low-dose imaging mode of the microscope: the electron dose (always below 150 $e$/nm$^2$) was kept minimal yet sufficient to record a micrograph. Micrographs were recorded digitally on a 2K CCD camera, using the DigitalMicrograph software.

## 4. RESULTS AND DISCUSSION

**4.1. Rheology in the Steady-Shear Regime.** The basic surfactant solution consists of CAPB and SLES in a 7:3 molar ratio. At this ratio and total surfactant (CAPB + SLES) concentration $c_{tot}$ = 100 mM, the natural pH is ca. 5.8 and the solution viscosity is maximal, $\eta_0$ = 2.3 mPa·s, because of the synergistic growth of cylindrical micelles.[62] In the present study, the focus is on the effect of fatty acid, which is added as a third component and is known to induce micellar growth.[33,35,57]

Figure 2 presents our results from the steady-shear experiments. The total surfactant concentration was fixed, $c_{tot}$ = 100 mM (70 mM CAPB + 30 mM SLES), whereas the HC8 concentration was varied from 0 to 30 mM. Figure 2a shows the dependence of the apparent viscosity $\eta$ on the shear rate $\dot{\gamma}$. As seen in the figure, the low-viscosity solutions behave as quasi-Newtonian fluids. Thus, the solution, which contains 12 mM HC8, is practically Newtonian over the whole range of shear rates from 0.1 to 10 $s^{-1}$.

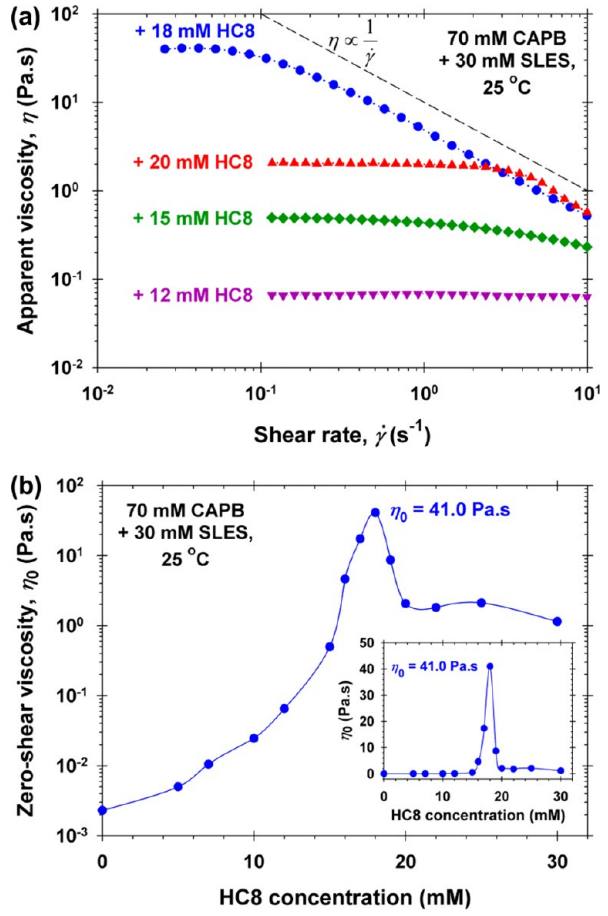


**Figure 2.** Effect of octanoic acid (HC8) on the sample's viscosity at fixed $c_{tot}$ = 100 mM (70 mM CAPB and 30 mM SLES); data are from the steady-shear regime. (a) Plot of the apparent shear viscosity $\eta$ vs the shear rate $\dot{\gamma}$. (b) Zero-shear viscosity $\eta_0$ vs HC8 concentration plotted on a semilog scale. The inset represents the same graph on a linear scale.

In contrast, as seen in Figure 2a, at 15, 18, and 20 mM HC8, the solutions remain Newtonian up to a certain threshold shear rate $\dot{\gamma}_N$, but at $\dot{\gamma} > \dot{\gamma}_N$ shear-thinning is observed. The switch



DOI: 10.1021/acs.langmuir.6b03955
Langmuir 2016, 32, 12885−12893

between Newtonian and shear-thinning behavior depends on the relaxation time $\tau_R$ and, as a rule, happens at lower $\dot{\gamma}_N$ for longer micelles. Indeed, at 18 mM HC8 and low shear rates, the micellar solution is highly viscoelastic ($\eta_0$ = 41.0 Pa·s) and then $\eta$ starts to decrease even at low shear rates $\dot{\gamma} \geq 0.1$ $s^{-1}$. Moreover, the rheological response at high shear rates, $\eta \propto \dot{\gamma}^{-1}$ at $\dot{\gamma} > \dot{\gamma}_N$, is characteristic for solutions of interwoven wormlike micelles.[10,33,39]

Figure 2b shows the dependence of the zero-shear viscosity $\eta_0$ on the HC8 concentration. Upon addition of HC8, $\eta_0$ passes through a sharp maximum at 18 mM HC8, reaching a maximal value of 41.0 Pa·s (Figure 2b). The maximum is 4 orders of magnitude higher than the viscosity (2.3 mPa·s) of the binary micellar solution without octanoic acid. A similar sharp peak in viscosity (rapid growth) was recently reported[35] for the same surfactants, CAPB and SLES, in the presence of lauric acid (HC12).

Typically, such viscous mixtures are either isotropic micellar solutions or liquid-crystalline mesophases. To check whether liquid-crystalline structures are present in the investigated solutions (Figure 2b), we used polarized-light optical microscopy and detected no birefringence. Hence, the ternary solutions are isotropic (micellar) up to 25 mM HC8. The pH of these micellar solutions decreases from 5.8 (no HC8) to about 5.1 (Figure S2a). At higher HC8 concentrations, the solutions become turbid because the excess fatty acid cannot be solubilized in the mixed micelles and precipitates in the form of small droplets; see Figure S2 and ref 63. Above 25 mM HC8, the pH levels off because the concentration of HC8 in the bulk is fixed at 4.2 mM, that is, the solubility of octanoic acid in water at 25 °C.[63]

It should be noted that it is HC8, rather than sodium carboxylate (NaC8), that induces the micellar growth. Indeed, as shown in Figure S2b, the degree of HC8 ionization in the mixed micelles is less than 4.5%. Moreover, if we interchange HC8 with NaC8, the viscosity $\eta_0$ decreases (Figure S3). The latter can be explained as follows: NaC8 increases the surface charge density of the mixed micelles. Hence, they diminish in size because of the increased intramicellar electrostatic repulsion between the negatively charged headgroups and $\eta_0$ drops. In contrast, the nonionic HC8 decreases the surface charge density of the mixed micelles and serves as a spacer between the negatively charged SLES headgroups, which leads to micellar growth.

Figure S4 shows our results from the steady-shear experiments at $c_{tot}$ = 200 mM (140 mM CAPB + 60 mM SLES). We see that by increasing $c_{tot}$ 2-fold the zero-shear viscosity $\eta_0$ at the peak increases ca. 10 times: from 41.0 Pa·s at $c_{tot}$ = 100 mM to 435 Pa.s at $c_{tot}$ = 200 mM. It should be noticed that the position of the peak shifts to the right from 18 mM HC8 at $c_{tot}$ = 100 mM to 25 mM HC8 at $c_{tot}$ = 200 mM. Counterintuitively, the position of the peak does not change in proportion to the total surfactant (CAPB + SLES) concentration $c_{tot}$: one would expect the peak to be at 36 mM HC8, but in reality it is at 25 mM HC8. Therefore, we studied the effect of $c_{tot}$ on the rheological behavior at a fixed ratio, 7:3 CAPB/SLES, and a fixed fatty acid concentration, 18 mM HC8, so that we always stay to the left of the viscosity peak.

In Figure 3, we illustrate the effect of $c_{tot}$ on the flow curves $\eta(\dot{\gamma})$ and on the zero-shear viscosity $\eta_0$. The flow curves in Figure 3a behave in a similar way to those in Figure 2a: at high shear rates, $\eta \propto \dot{\gamma}^{-1}$ at $\dot{\gamma} > \dot{\gamma}_N$. To visualize the effect of the total surfactant concentration, in Figure 3b we have plotted $\eta_0$ vs $c_{tot}$.

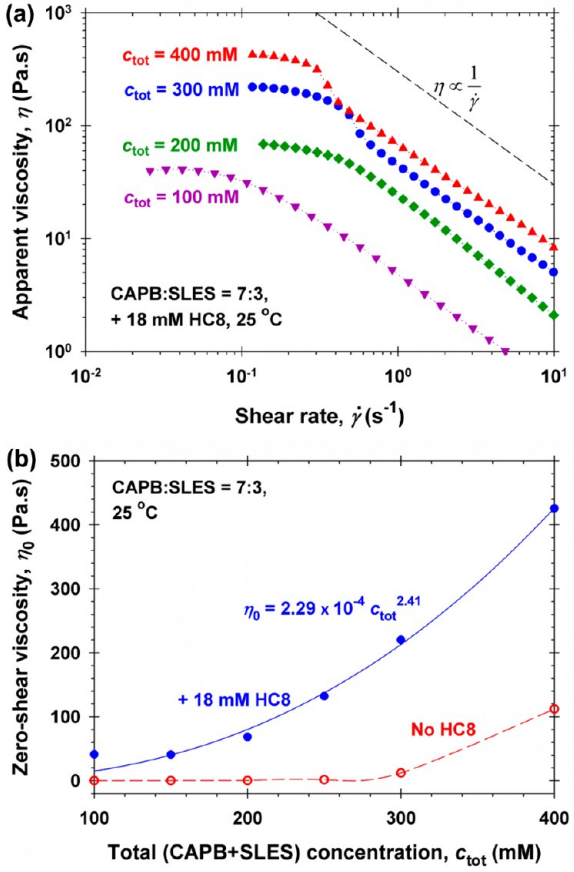


**Figure 3.** Effect of the total surfactant concentration $c_{tot}$ on the solution's viscosity at a fixed octanoic acid (HC8) concentration. (a) Plot of the apparent shear viscosity $\eta$ vs the shear rate $\dot{\gamma}$. (b) Zero-shear viscosity $\eta_0$ vs $c_{tot}$; the solid line is the best fit with a power-law dependence, whereas the dashed line is a guide to the eye.

We see that $\eta_0$ increases with the increase in $c_{tot}$, e.g., $\eta_0$ = 426 Pa·s at $c_{tot}$ = 400 mM vs $\eta_0 \approx$ 41 Pa·s at $c_{tot}$ = 100 mM. As shown in Figure 3b, the data obey a power-law dependence, $\eta_0 \propto c_{tot}^{2.4}$. The exponent 2.4 is intermediate between the values 1 and 2 measured for multiconnected micelles[12] and the values 3.5 and 3.7 for one-component wormlike micelles.[6,17] Additional data for the shear stress vs shear rate can be found in Figure S5.

**4.2. Rheology in the Oscillatory Regime.** Figure 4a shows plots of the storage and loss moduli, $G'$ and $G''$, versus the angular frequency, $\omega$, at a fixed shear-strain amplitude of 2%. For all experimental curves, the molar ratio CAPB/SLES is equal to 7:3, and the concentration of fatty acid is fixed at 18 mM HC8; the total surfactant concentration is $c_{tot}$ = 100 and 400 mM for the respective pairs of curves. The investigated micellar solutions are viscoelastic; they are fluidlike ($G'' > G'$) at low frequencies and solidlike at high frequencies ($G' > G''$). From the crossing point ($G' = G''$), one can determine the crossover frequency $\omega_c$ and estimate the relaxation time $\tau_R = 1/\omega_c$; see Section 2.

To determine $\tau_R$ in a more reliable way, we simultaneously fitted $G'(\omega)$ and $G''(\omega)$ up to the crossing point using the Maxwell model described by eq 2; see the solid lines in Figure 4a. The plateau modulus $G_0$ and the relaxation time $\tau_R$ were obtained as adjustable parameters from the fit. Analogous results for $c_{tot}$ = 200 and 300 mM can be found in Figure S6. The obtained values of $G_0$ and $\tau_R$ are given in the second and


DOI: 10.1021/acs.langmuir.6b03955
Langmuir 2016, 32, 12885−12893

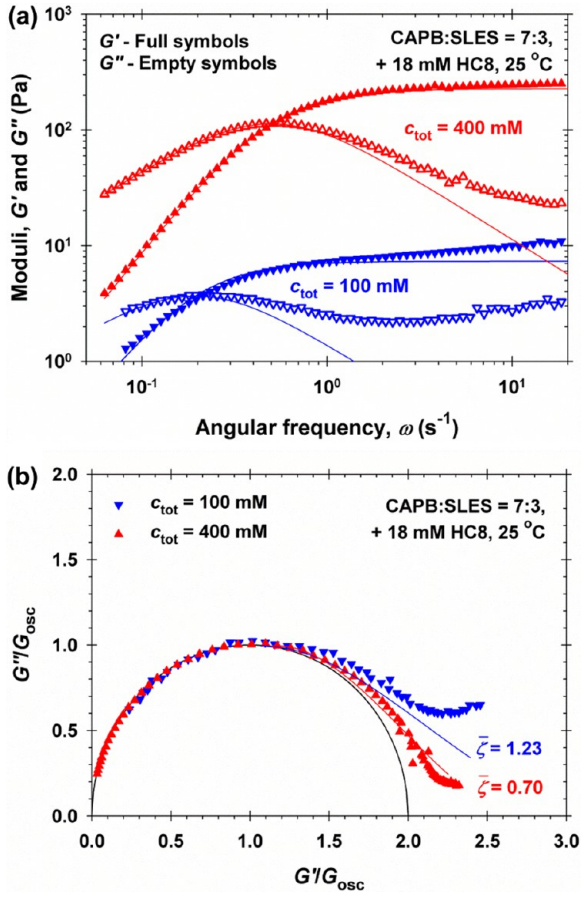


**Figure 4.** Rheological data in the oscillatory regime at $c_{tot}$ = 100 and 400 mM (CAPB + SLES) at the same 18 mM HC8 concentration. (a) Storage and loss moduli, $G'$ and $G''$, vs the angular frequency, $\omega$; the solid lines are drawn in accordance with the Maxwell model. (b) Cole–Cole plots of $G''/G_{osc}$ vs $G'/G_{osc}$, where $G_{osc} = G_0/2$; the semicircle represents pure Maxwellian behavior, whereas the solid lines are fits of the numerical data from refs 8 and 17.

third columns in Table 1. $G_0$ increases monotonically from 7.32 to 226 Pa as a function of $c_{tot}$, whereas $\tau_R$ decreases and reaches

**Table 1. Rheological Properties of the Studied Micellar Solutions at Fixed, 18 mM HC8 Concentration and Varying Total (CAPB + SLES) Concentration $c_{tot}$**

| $c_{tot}$ (mM) | $G_0$ (Pa) | $\tau_R$ (s) | $\xi$ (nm) | $\eta_{\omega=0}$ (Pa·s) | $\eta_0$ (Pa·s) | $\bar{\zeta}$ | $\tau_{break}$ (s) |
|---|---|---|---|---|---|---|---|
| 100 | 7.32 | 5.15 | 82.5 | 37.7 | 41.0 | 1.23 | 6.33 |
| 200 | 30.6 | 1.95 | 51.2 | 59.7 | 68.5 | 4.61 | 8.99 |
| 300 | 113 | 2.03 | 33.1 | 229 | 220 | 1.23 | 2.50 |
| 400 | 226 | 1.99 | 26.3 | 450 | 426 | 0.70 | 1.39 |

a plateau of ca. 2 s at the higher total surfactant concentrations. It is interesting that $G_0(c_{tot})$ follows a power-law dependence with an exponent of 2.5, which is in good agreement with the value of 2.3 ± 0.2 expected from refs 6 and 17 as well as with the value of 2.25 determined in ref 64.

Using the values of $G_0$ and eq 4, we calculated the correlation length $\xi$, which is an estimate of the mesh size of the transient micellar network; see Table 1. $\xi$ decreases about 3-fold, from about 83 to 26 nm, as the wormlike micellar solutions become more concentrated. By substituting $G_0$ and $\tau_R$ into eq 4, we also estimated the zero-frequency viscosity $\eta_{\omega=0}$. In the fifth and sixth columns of Table 1, the values of $\eta_{\omega=0}$ and $\eta_0$ are compared. ($\eta_0$ is the plateau value of $\eta$ at low $\dot{\gamma}$ obtained from the steady-shear experiments; see above.) In all cases, $\eta_{\omega=0}$ and $\eta_0$ coincide within 12%, which is known as the Cox–Merz rule in the polymer literature.[59,65]

To obtain quantitative information about the stress relaxation mechanisms (breaking and reptation), we determined the parameter $\bar{\zeta}$, which is related to $\tau_{break}$; see eq 6. The procedure is as follows: (1) The experimental data are plotted on the dimensionless scale $G''/G_{osc}$ vs $G'/G_{osc}$ (a Cole–Cole plot). For pure Maxwellian behavior (eq 5), the Cole–Cole plot represents a semicircle of radius $G_{osc} = G_0/2$. If there are deviations from the semicircle, they typically occur at high frequencies (high $G'$) and are quantified by $\bar{\zeta}$. (2) To determine $\bar{\zeta}$, the experimental Cole–Cole plots are compared to the theoretical Cole–Cole plots (for $\bar{\zeta}$ = 0.13, 0.38, 0.70, 1.23, 2.38, 4.61 and 10.2) given in refs 8 and 17. (3) From this comparison, the value of $\bar{\zeta}$ that best describes our rheological data is determined, and $\tau_{break} = \bar{\zeta}\tau_R$ (eq 6) is calculated.

Figure 4b presents the Cole–Cole plots for $c_{tot}$ = 100 and 400 mM. Analogous plots for $c_{tot}$ = 200 and 300 mM are given in Figure S7. In Figures 4b and S7, our rheological data (symbols) are compared with the theoretical Cole–Cole plots (solid lines) from refs 8 and 17. From this comparison, the estimated values of $\bar{\zeta}$ are given in Table 1, where the last column contains the values of the characteristic time for reversible scission, $\tau_{break}$. In other words, we estimated $\tau_{break}$ from purely rheological data using Cates' model.[8] (For concentrated surfactant systems, $\tau_{break}$ is difficult to measure directly via T-jump experiments.) Cates' model predicts that $\tau_{break}$ is inversely proportional to the average micellar length $\bar{L}$. Typically, $\bar{L} \propto (c_{tot})^{1/2}$, e.g., refs 1 and 35. Hence, $\tau_{break}$ is expected to decrease with the increase in $c_{tot}$, in agreement with the tendency of our data in Table 1.

**4.3. Cryo-TEM Imaging.** Cryogenic TEM was applied to obtain structure-specific information for the changes that occur in the investigated micellar solutions at $c_{tot}$ = 100 mM and increasing HC8 concentration. At higher $c_{tot}$, the cryo-TEM imaging is cumbersome, mainly for two reasons: (i) a thin sample (below 250 nm) is difficult to prepare and (ii) the micrographs become crowded because of overlapping micelles. Cryo-TEM micrographs were taken at the viscosity peak, 18 mM HC18, and on both sides of the peak, viz., at 15 and 20 mM HC8; see Figure 2b.

Figure 5 shows typical cryo-TEM micrographs taken at 15 mM HC8, i.e., to the left of the peak, where the zero-shear viscosity is $\eta_0$ = 496 mPa·s. Under these conditions, long overlapping wormlike micelles are seen throughout the sample. The micelles are highly polydisperse in length, which is typical for cylindrical and wormlike aggregates. The solution's viscosity is nearly 500 times that of water because the worms are hundreds of nanometers in length and have a high length-to-thickness aspect ratio. Such elongated micelles can easily overlap and enhance the rheological response of the system.

Figure 6 shows micrographs taken at the viscosity peak, at 18 mM HC8, where the viscosity is $\eta_0 \approx$ 41 000 mPa·s. Figure 6a represents a large area populated with giant intertwined wormlike micelles. Figure 6a,b shows that the micelles reach micrometer lengths so that their length-to-thickness aspect ratio exceeds 200. The latter is among the primary reasons for high solution viscosity and gel-like structure because the worms start to entangle and form a transient micellar network.



DOI: 10.1021/acs.langmuir.6b03955
Langmuir 2016, 32, 12885–12893

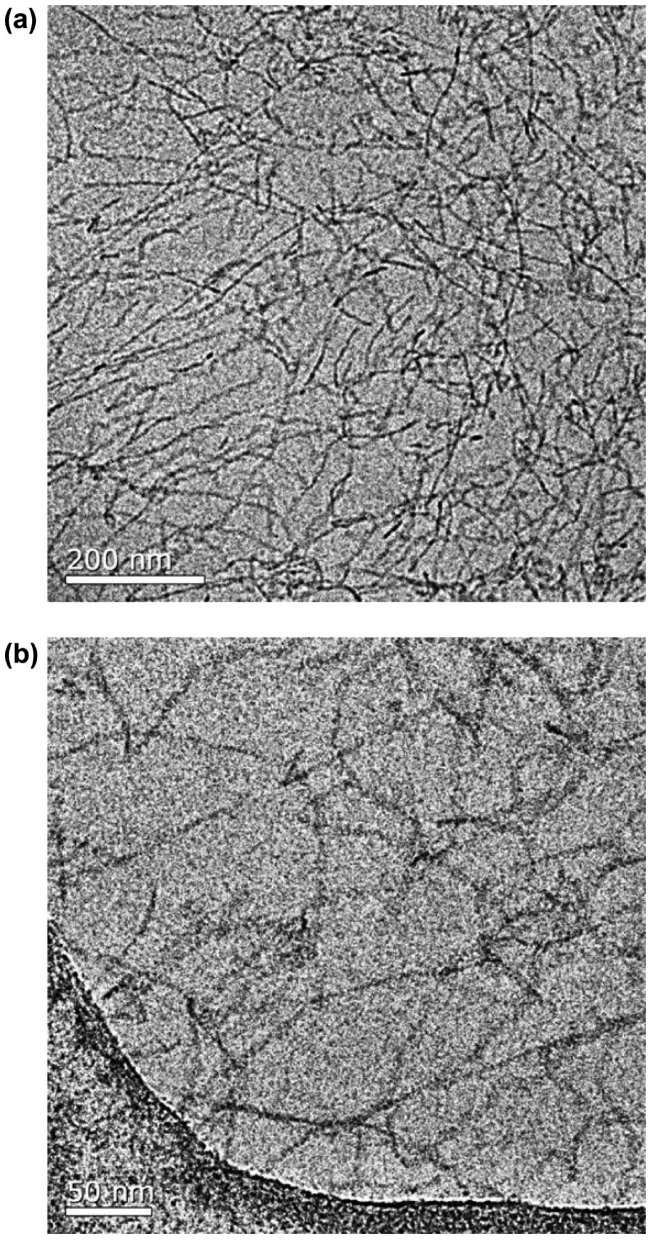


**Figure 5.** Cryo-TEM micrographs at 15 mM HC8 (to the left of the viscosity peak), 70 mM CAPB, and 30 mM SLES, with $\eta_0$ = 0.496 Pa·s. (a) Long polydisperse wormlike micelles form a dense film of superimposed structures (200 nm scale bar). (b) The wormlike micelles are hundreds of nanometers long with a thickness of up to 5−6 nm (50 nm scale bar).

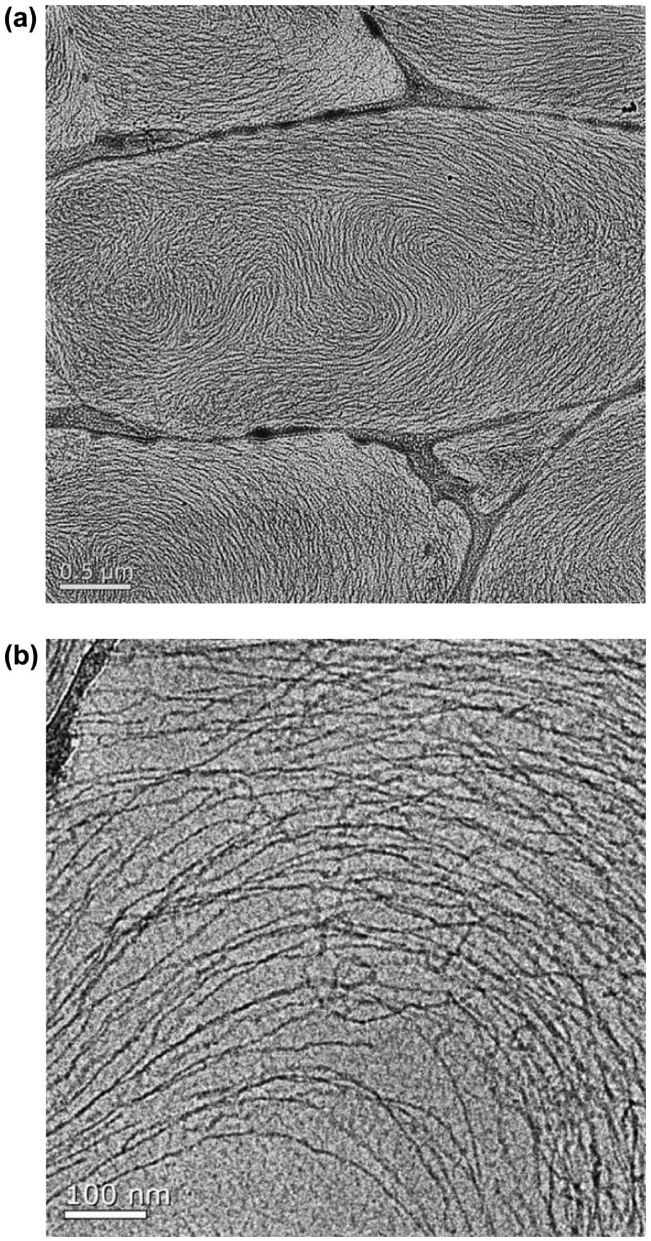


**Figure 6.** Cryo-TEM micrographs at 18 mM HC8 (at the viscosity peak), 70 mM CAPB, and 30 mM SLES, with $\eta_0$ = 41.0 Pa·s. (a) Giant interwoven wormlike micelles, which reach micrometer lengths, are observed on large areas of the grid (500 nm scale bar). (b) The wormlike micelles are entangled, but they do not seem to form junctions and loops (100 nm scale bar).

It is important to note, however, that the micellar network is not interconnected; neither 3-fold and 4-fold junctions nor loops are seen in Figure 6b. All apparent crossing points are actually superimposed micelles from different planes, which overlap in the two-dimensional snapshot. Thus, it turns out that the sharp peak in viscosity (Figure 2b) is due to the formation of giant intertwined wormlike micelles.

Figure 7 presents cryo-TEM micrographs taken at 20 mM HC8, i.e., to the right of the peak, where the viscosity is $\eta_0$ = 2060 mPa·s. One sees that (i) the wormlike micelles are organized in bundles (Figure 7a) and (ii) the individual wormlike micelles coexist with multiconnected micelles and small rings (loops); see Figure 7b. Such structures as well as branched micelles, in general, are known to have additional stress relief mechanisms available, viz., the fast and fluid sliding of branch points along the micelles and ghostlike crossings at 4-fold junctions.[11,12,55,56] These molecular mechanisms can explain the observed drop in viscosity to the right of the peak (Figure 2b) as well as the rheological data in Table S1. It should be mentioned that branching in mixed systems is rather common and could be due to local inhomogeneities in the micelle composition.[54]

## 5. CONCLUSIONS

In the present article, we investigated the synergistic growth of giant wormlike micelles in ternary mixed solutions, which consist of anionic (SLES), zwitterionic (CAPB), and nonionic



DOI: 10.1021/acs.langmuir.6b03955
*Langmuir* 2016, 32, 12885−12893

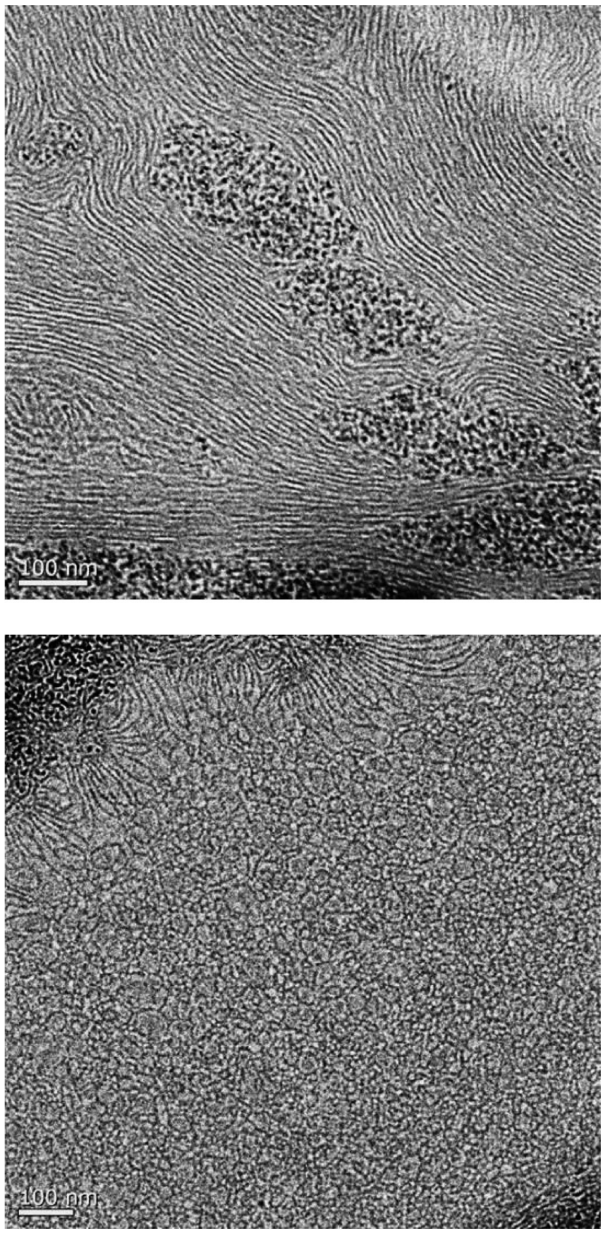


**Figure 7.** Cryo-TEM micrographs at 20 mM HC8 (to the right of the viscosity peak), 70 mM CAPB, and 30 mM SLES, with $\eta_0$ = 2.06 Pa·s (100 nm scale bars). (a) Long wormlike micelles organized in bundles; the areas with black dots represent cross sections of such bundles. (b) Wormlike structures coexist with multiconnected micelles and small rings.

(HC8) surfactants. The effect of cosurfactant (HC8) on solution rheology and phase behavior was studied at a fixed 7:3 CAPB/SLES molar ratio. Similar to other worm-forming formulations,[2−4,13,18−24,29−35,38−40,42,44−46] the viscosity of the mixtures $\eta_0$ follows a nonmonotonic trend. In our case, a sharp and high peak with $\eta_0 \approx$ 41 000 mPa·s at 18 mM HC8 (Figure 2b) was detected, which is 4 orders of magnitude greater than the viscosity of the binary surfactant solution without HC8.

Using optical microscopy in transmitted-light polarization mode, we did not detect any birefringence, which directly proves that all ternary solutions up to 25 mM HC8 are isotropic micellar rather than liquid-crystalline. In contrast to the similar system studied in ref 57, we can exclude the transition from isotropic micellar solution to the liquid-crystalline phase as a probable explanation of the origin of the viscosity peak.

The steady-state and oscillatory rheological experiments show that the investigated ternary micellar solutions are viscoelastic and obey the Maxwell viscoelastic model in a wide range of shear rates. At high rates of strain, the shear stress levels off (shear-banding) and $\eta \propto \dot{\gamma}^{-1}$, which is typical for solutions with intertwined wormlike micelles.[10,33,39] However, the shear-banding response and Maxwellian behavior have also been observed with solutions containing disclike micelles.[57] Therefore, to directly obtain structure-specific information and to identify the microstructures behind the nonmonotonic rheological behavior, we employed cryogenic TEM.

The cryo-TEM imaging revealed complex phase behavior: wormlike micelles to the left of the peak, giant entangled wormlike micelles at the peak, and wormlike micelles coexisting with multiconnected micelles to the right of the peak. In mixed micellar solutions, multiconnected micelles could form as a result of local inhomogeneities in the micelle composition. Such multiconnected networks provide stress relief mechanisms analogous to those typical for branched micelles,[11,12,55,56] whose formation is typically associated with the viscosity reduction to the right of the peak (Figure 2b).

For the first time in the present article, SLES-CAPB-fatty acid mixtures are studied in detail by both rheological and cryo-TEM measurements, even though these ternary mixtures are widely used in many industrial products such as shampoo and body wash. Furthermore, the results contribute to the understanding of the structure−rheology relation in mixed micellar solutions containing giant micelles. It is demonstrated that small changes in the micelle composition and cosurfactant charge (HC8 vs NaC8), which affect the molecular packing within the micelle and the intramicellar interactions, could produce a rapid growth of wormlike micelles that leads to a drastic change in both the solution rheology and microstructure. This effect could be utilized to control the physicochemical and rheological properties of surfactant formulations with applications in personal care and household detergency, including the preparation of low-surfactant formulations, thus, decreasing the contamination of the environment by detergents.

## ■ ASSOCIATED CONTENT

### Supporting Information

The Supporting Information is available free of charge on the ACS Publications website at DOI: 10.1021/acs.langmuir.6b03955.

Additional experimental and numerical results (PDF)

## ■ AUTHOR INFORMATION

### Corresponding Author

*Phone (+359) 2-8161262. Fax (+359) 2-9625643. E-mail: pk@lcpe.uni-sofia.bg.

### Notes

The authors declare no competing financial interest.

## ■ ACKNOWLEDGMENTS

The authors gratefully acknowledge the support from EU COST Action CM1101 and the Horizon 2020 project ID: 692146-H2020-eu.4.b "Materials Networking". S.E.A. is especially grateful for the travel grant from FP7 project Beyond-Everest for the research visit to Max Planck Institute for



DOI: 10.1021/acs.langmuir.6b03955
*Langmuir* 2016, 32, 12885−12893

Polymer Research, Mainz, Germany. The authors thank Prof. Krassimir Danov (Sofia University) for the critical reading of the article. We are grateful to Prof. Heinz Hoffmann (Bayreuth University) and Prof. Dganit Danino (Technion − IIT, Haifa) for their valuable comments and helpful discussions.

## REFERENCES

(1) Israelachvili, J. N. *Intermolecular and Surface Forces*; Academic Press: London, 2011.
(2) Rehage, H.; Hoffmann, H. Rheological properties of viscoelastic surfactant systems. *J. Phys. Chem.* **1988**, *92*, 4712−4719.
(3) Rehage, H.; Hoffmann, H. Viscoelastic surfactant solutions: Model systems for rheological research. *Mol. Phys.* **1991**, *74*, 933−973.
(4) Clausen, T. M.; Vinson, P. K.; Minter, J. R.; Davis, H. T.; Talmon, Y.; Miller, W. G. Viscoelastic micellar solutions: microscopy and rheology. *J. Phys. Chem.* **1992**, *96*, 474−484.
(5) Cates, M. E. Reptation of living polymers: Dynamics of entangled polymers in the presence of reversible chain-scission reactions. *Macromolecules* **1987**, *20*, 2289−2296.
(6) Cates, M. E.; Candau, S. J. Statics and dynamics of worm-like surfactant micelles. *J. Phys.: Condens. Matter* **1990**, *2*, 6869−6892.
(7) Cates, M. E. Nonlinear viscoelasticity of wormlike micelles (and other reversibly breakable polymers). *J. Phys. Chem.* **1990**, *94*, 371−375.
(8) Turner, M. S.; Cates, M. E. Linear viscoelasticity of living polymers: A quantitative probe of chemical relaxation times. *Langmuir* **1991**, *7*, 1590−1594.
(9) Granek, R.; Cates, M. E. Stress relaxation in living polymers: Results from a Poisson renewal model. *J. Chem. Phys.* **1992**, *96*, 4758−4767.
(10) Spenley, N. A.; Cates, M. E.; McLeish, T. C. B. Nonlinear rheology of wormlike micelles. *Phys. Rev. Lett.* **1993**, *71*, 939−942.
(11) Lequeux, F. Reptation of connected wormlike micelles. *Europhys. Lett.* **1992**, *19*, 675−681.
(12) Khatory, A.; Kern, F.; Lequeux, F.; Appell, J.; Porte, G.; Morie, N.; Ott, A.; Urbach, W. Entangled versus multiconnected network of wormlike micelles. *Langmuir* **1993**, *9*, 933−939.
(13) Candau, S. J.; Oda, R. Linear viscoelasticity of salt-free wormlike micellar solutions. *Colloids Surf., A* **2001**, *183−185*, 5−14.
(14) Magid, L. J. The surfactant−polyelectrolyte analogy. *J. Phys. Chem. B* **1998**, *102*, 4064−4074.
(15) Dreiss, C. A. Wormlike micelles: where do we stand? Recent developments, linear rheology and scattering techniques. *Soft Matter* **2007**, *3*, 956−970.
(16) Yang, J. Viscoelastic wormlike micelles and their applications. *Curr. Opin. Colloid Interface Sci.* **2002**, *7*, 276−281.
(17) Kern, F.; Lemarechal, P.; Candau, S. J.; Cates, M. E. Rheological properties of semidilute and concentrated solutions of cetyltrimethylammonium bromide in the presence of potassium bromide. *Langmuir* **1992**, *8*, 437−440.
(18) Candau, S. J.; Khatory, A.; Lequeux, F.; Kern, F. Rheological behaviour of wormlike micelles: effect of salt content. *J. Phys. IV* **1993**, *3*, C1-197−C1-209.
(19) Ali, A. A.; Makhloufi, R. Linear and nonlinear rheology of an aqueous concentrated system of cethyltrimethylammonium chloride and sodium salicylate. *Phys. Rev. E: Stat. Phys., Plasmas, Fluids, Relat. Interdiscip. Top.* **1997**, *56*, 4474−4478.
(20) Hartmann, V.; Cressely, R. Linear and non-linear rheology of a wormlike micellar system in presence of sodium tosylate. *Rheol. Acta* **1998**, *37*, 115−121.
(21) Aswal, V. K.; Goyal, P. S.; Thiyagarajan, P. Small-angle neutron-scattering and viscosity studies of CTAB/NaSal viscoelastic micellar solutions. *J. Phys. Chem. B* **1998**, *102*, 2469−2473.
(22) Cappelaere, E.; Cressely, R. Influence of $NaClO_3$ on the rheological behaviour of a micellar solution of CPCl. *Rheol. Acta* **2000**, *39*, 346−353.
(23) Croce, V.; Cosgrove, T.; Maitland, G.; Hughes, T.; Karlsson, G. Rheology, cryogenic transmission electron spectroscopy, and small-angle neutron scattering of highly viscoelastic wormlike micellar solutions. *Langmuir* **2003**, *19*, 8536−8541.
(24) Angelescu, D.; Khan, A.; Caldararu, H. Viscoelastic properties of sodium dodecyl sulfate with aluminum salt in aqueous solution. *Langmuir* **2003**, *19*, 9155−9161.
(25) Raghavan, S. R.; Kaler, E. W. Highly viscoelastic wormlike micellar solutions formed by cationic surfactants with long unsaturated tails. *Langmuir* **2001**, *17*, 300−306.
(26) Oelschlaeger, C.; Waton, G.; Buhler, E.; Candau, S. J.; Cates, M. E. Rheological and light scattering studies of cationic fluorocarbon surfactant solutions at low ionic strength. *Langmuir* **2002**, *18*, 3076−3085.
(27) Saul, D.; Tiddy, G. J. T.; Wheeler, B. A.; Wheeler, P. A.; Willis, E. Phase structure and rheological properties of a mixed zwitterionic/anionic surfactant system. *J. Chem. Soc., Faraday Trans. 1* **1974**, *70*, 163−170.
(28) Kumar, S.; Aswal, V. K.; Singh, H. N.; Goyal, P. S. Growth of sodium dodecyl sulfate micelles in the presence of n-octylamine. *Langmuir* **1994**, *10*, 4069−4072.
(29) Hoffmann, H.; Rauscher, A.; Gradzielski, M.; Schulz, S. F. Influence of ionic surfactants on the viscoelastic properties of zwitterionic surfactant solutions. *Langmuir* **1992**, *8*, 2140−2146.
(30) Acharya, D. P.; Hattori, K.; Sakai, T.; Kunieda, H. Phase and rheological behavior of salt-free alkyltrimethylammonium bromide/alkanoyl-N-methylethanolamide/water systems. *Langmuir* **2003**, *19*, 9173−9178.
(31) Afifi, H.; Karlsson, G.; Heenan, R. K.; Dreiss, C. A. Solubilization of oils or addition of monoglycerides drives the formation of wormlike micelles with an elliptical cross-section in cholesterol-based surfactants: A study by rheology, SANS, and cryo-TEM. *Langmuir* **2011**, *27*, 7480−7492.
(32) Parker, A.; Fieber, W. Viscoelasticity of anionic wormlike micelles: effects of ionic strength and small hydrophobic molecules. *Soft Matter* **2013**, *9*, 1203−1213.
(33) Mitrinova, Z.; Tcholakova, S.; Popova, J.; Denkov, N.; Dasgupta, B.; Ananthapadmanabhan, K. P. Efficient control of the rheological and surface properties of surfactant solutions containing C8−C18 fatty acids as cosurfactants. *Langmuir* **2013**, *29*, 8255−8265.
(34) Kamada, M.; Shimizu, S.; Aramaki, K. Manipulation of the viscosity behavior of wormlike micellar gels by changing the molecular structure of added perfumes. *Colloids Surf., A* **2014**, *458*, 110−116.
(35) Anachkov, S. E.; Kralchevsky, P. A.; Danov, K. D.; Georgieva, G. S.; Ananthapadmanabhan, K. P. Disclike vs. cylindrical micelles: generalized model of micelle growth and data interpretation. *J. Colloid Interface Sci.* **2014**, *416*, 258−273.
(36) Kaler, E. W.; Herrington, K. L.; Murthy, A. K.; Zasadzinski, J. A. N. Phase behavior and structures of mixtures of anionic and cationic surfactants. *J. Phys. Chem.* **1992**, *96*, 6698−6707.
(37) Brasher, L. L.; Herrington, K. L.; Kaler, E. W. Electrostatic effects on the phase behavior of aqueous cetyltrimethylammonium bromide and sodium octyl sulfate mixtures with added sodium bromide. *Langmuir* **1995**, *11*, 4267−4277.
(38) Koehler, R. D.; Raghavan, S. R.; Kaler, E. W. Microstructure and dynamics of wormlike micellar solutions formed by mixing cationic and anionic surfactants. *J. Phys. Chem. B* **2000**, *104*, 11035−11044.
(39) Raghavan, S. R.; Fritz, G.; Kaler, E. W. Wormlike micelles formed by synergistic self-assembly in mixtures of anionic and cationic surfactants. *Langmuir* **2002**, *18*, 3797−3803.
(40) Ziserman, L.; Abezgauz, L.; Ramon, O.; Raghavan, S. R.; Danino, D. Origins of the viscosity peak in wormlike micellar solutions. 1. Mixed catanionic surfactants. A cryo-transmission electron microscopy study. *Langmuir* **2009**, *25*, 10483−10489.
(41) Schubert, B. A.; Kaler, E. W.; Wagner, N. J. The microstructure and rheology of mixed cationic/anionic wormlike micelles. *Langmuir* **2003**, *19*, 4079−4089.
(42) Kern, F.; Lequeux, F.; Zana, R.; Candau, S. J. Dynamic properties of salt-free viscoelastic micellar solutions. *Langmuir* **1994**, *10*, 1714−1723.



DOI: 10.1021/acs.langmuir.6b03955
*Langmuir* 2016, 32, 12885−12893

(43) Bernheim-Groswasser, A.; Zana, R.; Talmon, Y. Sphere-to-cylinder transition in aqueous micellar solution of a dimeric (gemini) surfactant. *J. Phys. Chem. B* **2000**, *104*, 4005−4009.
(44) Acharya, D. P.; Kunieda, H.; Siba, Y.; Aratani, K. Phase and rheological behavior of novel gemini-type surfactant systems. *J. Phys. Chem. B* **2004**, *108*, 1790−1797.
(45) Acharya, D. P.; Khalid Hossain, Md.; Feng, J.; Sakai, T.; Kunieda, H. Phase and rheological behavior of viscoelastic wormlike micellar solutions formed in mixed nonionic surfactant systems. *Phys. Chem. Chem. Phys.* **2004**, *6*, 1627−1631.
(46) Naito, N.; Acharya, D. P.; Tanimura, J.; Kunieda, H. Rheological behavior of wormlike micellar solutions in mixed nonionic systems of polyoxyethylene phytosterol-polyoxyethylene dodecyl ether. *J. Oleo Sci.* **2004**, *53*, 599−606.
(47) Moitzi, C.; Freiberger, N.; Glatter, O. Viscoelastic wormlike micellar solutions made from nonionic surfactants: Structural investigations by SANS and DLS. *J. Phys. Chem. B* **2005**, *109*, 16161−16168.
(48) Kusano, T.; Iwase, H.; Yoshimura, T.; Shibayama, M. Structural and rheological studies on growth of salt-free wormlike micelles formed by star-type trimeric surfactants. *Langmuir* **2012**, *28*, 16798−16806.
(49) Hoffmann, H. Viscoelastic surfactant solutions. In *Structure and Flow in Surfactant Solutions*; Herb, C. A., Prud'homme, R. K., Eds.; ACS Symposium Series 578; American Chemical Society: Washington, DC, 1994; pp 2−31.
(50) Singh, M.; Ford, C.; Agarwal, V.; Fritz, G.; Bose, A.; John, V. T.; McPherson, G. L. Structural evolution in cationic micelles upon incorporation of a polar organic dopant. *Langmuir* **2004**, *20*, 9931−9937.
(51) Couillet, I.; Hughes, T.; Maitland, G.; Candau, F.; Candau, S. J. Growth and scission energy of wormlike micelles formed by a cationic surfactant with long unsaturated tails. *Langmuir* **2004**, *20*, 9541−9550.
(52) Miyake, M.; Einaga, Y. Characteristics of wormlike pentaoxyethylene decyl ether C10E5 micelles containing n-dodecanol. *J. Phys. Chem. B* **2007**, *111*, 535−542.
(53) Afifi, H.; Karlsson, G.; Heenan, R. K.; Dreiss, C. A. Structural transitions in cholesterol-based wormlike micelles induced by encapsulating alkyl ester oils with varying architecture. *J. Colloid Interface Sci.* **2012**, *378*, 125−134.
(54) Danino, D. Cryo-TEM of soft molecular assemblies. *Curr. Opin. Colloid Interface Sci.* **2012**, *17*, 316−329.
(55) Appell, J.; Porte, G.; Khatory, A.; Kern, F.; Candau, S. Static and dynamic properties of a network of wormlike surfactant micelles (cetylpyridinium chlorate in sodium chlorate brine). *J. Phys. II* **1992**, *2*, 1045−1052.
(56) Drye, T. J.; Cates, M. E. Living networks: The role of cross-links in entangled surfactant solutions. *J. Chem. Phys.* **1992**, *96*, 1367−1375.
(57) Colafemmina, G.; Recchia, R.; Ferrante, A. S.; Amin, S.; Palazzo, G. Lauric acid-induced formation of a lyotropic nematic phase of disk-shaped micelles. *J. Phys. Chem. B* **2010**, *114*, 7250−7260.
(58) Cates, M. E.; Fielding, S. M. Rheology of giant micelles. *Adv. Phys.* **2006**, *55*, 799−879.
(59) Larson, R. G. *The Structure and Rheology of Complex Fluids*; Oxford University Press: Oxford, 1999.
(60) Murphy, D. B.; Davidson, M. W. *Fundamentals of Light Microscopy and Electronic Imaging*; Wiley-Blackwell: NJ, 2012.
(61) Danino, D.; Bernheim-Groswasser, A.; Talmon, Y. Digital cryogenic transmission electron microscopy: an advanced tool for direct imaging of complex fluids. *Colloids Surf., A* **2001**, *183-185*, 113−122.
(62) Christov, N. C.; Denkov, N. D.; Kralchevsky, P. A.; Ananthapadmanabhan, K. P.; Lips, A. Synergistic sphere-to-rod micelle transition in mixed solutions of sodium dodecyl sulfate and cocoamidopropyl betaine. *Langmuir* **2004**, *20*, 565−571.
(63) Tzocheva, S. S.; Kralchevsky, P. A.; Danov, K. D.; Georgieva, G. S.; Post, A. J.; Ananthapadmanabhan, K. P. Solubility limits and phase diagrams for fatty acids in anionic (SLES) and zwitterionic (CAPB) micellar surfactant solutions. *J. Colloid Interface Sci.* **2012**, *369*, 274−286.
(64) Oda, R.; Narayanan, J.; Hassan, P. A.; Manohar, C.; Salkar, R. A.; Kern, F.; Candau, S. J. Effect of the lipophilicity of the counterion on the viscoelasticity of micellar solutions of cationic surfactants. *Langmuir* **1998**, *14*, 4364−4372.
(65) Cox, W. P.; Merz, E. H. Correlation of dynamic and steady flow viscosities. *J. Polym. Sci.* **1958**, *28*, 619−622.


DOI: 10.1021/acs.langmuir.6b03955
*Langmuir* 2016, 32, 12885−12893

# Supporting Information

for the article

## Synergistic growth of giant wormlike micelles in ternary mixed surfactant solutions: Effect of octanoic acid

Gergana S. Georgieva,[†] Svetoslav E. Anachkov,[†] Ingo Lieberwirth,[‡] Kaloian Koynov,[‡], Peter A. Kralchevsky*,[†]

[†] *Department of Chemical and Pharmaceutical Engineering, Faculty of Chemistry and Pharmacy, Sofia University, 1 James Bourchier Blvd., 1164 Sofia, Bulgaria*

[‡] *Max Planck Institute for Polymer Research, 10 Ackermannweg, 55128 Mainz, Germany*

* *E-mail address*: pk@lcpe.uni-sofia.bg (P.A. Kralchevsky)

## Appendix A. Additional experimental and numerical results

### A.1. Electrolytic conductivity measurements of TEGO® Betain F50 salt content

From the product specification data of TEGO® Betain F50 (Goldschmidt GmbH – now part of Evonik Industries AG), one can see its chemical composition: CAPB (37 – 42 wt%), NaCl (5.8 – 7.3 wt%) and water.[1] In other words, 100 mM CAPB solution contains from 81 to 120 mM NaCl. To determine the exact amount of NaCl in our batch of TEGO® Betain F50, we carried out electrolytic conductivity measurements using a conductivity meter EC 215 (Hanna Instruments – USA).

Figure S1 shows that the electrolytic conductivity $\kappa$ increases as a function of CAPB concentration $c_{\mathrm{CAPB}}$. At its natural pH = 5.0 ± 0.5,[1] CAPB is in zwitterionic (uncharged) form, meaning that the observed increase of $\kappa$ is solely due to the presence of NaCl, given by:

$$c_{\mathrm{NaCl}} = x c_{\mathrm{CAPB}}\,, \tag{A.1}$$

where $c_{\mathrm{NaCl}}$ is the molar concentration of NaCl and $x$ is the molar fraction of salt with respect to CAPB. Then, the conductivity $\kappa$ of the studied solutions can be evaluated as follows:[2,3]

$$\kappa = \kappa_0 + \Lambda^{(0)}_{\mathrm{NaCl}} f(I) c_{\mathrm{NaCl}}\,. \tag{A.2}$$

Here, $\kappa_0$ is the background conductivity, which accounts for trace amounts of other ionic species (like $H^+$, $OH^-$, $HCO_3^-$) in the water used; $\Lambda^{(0)}_{\mathrm{NaCl}} = 126.39\ \mathrm{cm^2 \cdot S \cdot mol^{-1}}$ is the molar conductivity of NaCl solution at infinite dilution;[4] $f(I)$ is a correction coefficient for ion-ion interactions; and $I = c_{\mathrm{NaCl}}$, expressed as mol/L ≡ M, is the ionic strength. The correction factor $f(I)$ reads:[3]

$$f(I) = 1 - 0.7\sqrt{I} + 0.74I \,. \qquad \text{(A.3)}$$

Using eq A.2, we fitted the experimental data shown in Fig. S1. From the fit, $\kappa_0$ and $x$ were determined as adjustable parameters, and are as follows: $\kappa_0 = 6.5 \pm 1.3$ μS·cm$^{-1}$, close to that of water equilibrated with $CO_2$, and $x = 1.18 \pm 0.06$. In the latter value, we have taken into account that the typical error of the conductivity measurement is up to 5 %.

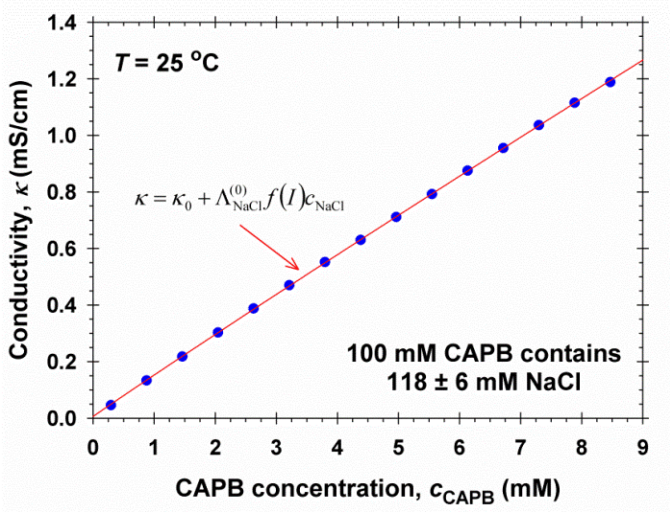


**Figure S1.** Plot of the electrolytic conductivity $\kappa$ versus CAPB concentration $c_{CAPB}$. The full circles represent the experimental data, whereas the solid line is the fit to the data using eq A.2.

### A.2. Ionization states of CAPB and HC8

First, we will discuss the ionization state of CAPB since it is a pH-sensitive molecule. As mentioned above, at pH = 5.0, CAPB is predominantly in zwitterionic (uncharged) form. There is only a trace amount of cationic-CAPB (c-CAPB), which can be calculated in the following way:

$$K_{a,c-CAPB} = \frac{a_{H^+} a_{CAPB}}{a_{c-CAPB}} \approx \frac{a_{H^+} c_{CAPB}}{c_{c-CAPB}} \Rightarrow \frac{c_{c-CAPB}}{c_{CAPB}} = \frac{10^{-pH}}{K_{a,c-CAPB}} \,. \qquad \text{(A.4)}$$

Here, $a_{H+}$, $a_{CAPB}$ and $a_{c\text{-}CAPB}$ are the activities of the respective species; and $K_{a,c\text{-}CAPB}$ is the acidity constant of c-CAPB. In eq A.4, we have assumed that the activity coefficients $\gamma_{CAPB}$ and $\gamma_{c\text{-}CAPB}$ are equal. For similar 1-12 carboxylate betaine, $K_{a,c\text{-}CAPB} \approx 10^{-2}$ M at 25 °C.[5] Therefore, using eq A.4, we estimate that c-CAPB should be around 0.1 % at pH = 5 and even less at higher pH.

Second, we will estimate the degree of HC8 ionization in the mixed micelles $\alpha$, consisting of CAPB, SLES and HC8. Following the approach from ref. 6, we have that:

$$\gamma_i y_i = \frac{c_i}{K_{i,\mathrm{mic}}}, \qquad (i = \mathrm{HC8 \text{ or } C8^-}). \tag{A.5}$$

Here, $\gamma_i$ and $y_i$ are the activity coefficient and the molar fraction of component $i$ in the micelles, respectively; $c_i$ is the respective monomer concentration in the bulk; and $K_{i,\mathrm{mic}}$ is the micellization constant, which is related to the work for transferring of a monomer of component $i$ from the solution into a micelle. Assuming that $\gamma_{\mathrm{HC8}} \approx \gamma_{\mathrm{C8}^-}$, from eq A.5, we obtain the relationship:

$$\frac{y_{\mathrm{C8}^-}}{y_{\mathrm{HC8}}} = \frac{c_{\mathrm{C8}^-}}{c_{\mathrm{HC8}}} \frac{K_{\mathrm{HC8,mic}}}{K_{\mathrm{C8}^-,\mathrm{mic}}}, \tag{A.6}$$

where $K_{\mathrm{HC8,mic}} \approx 3.7 \times 10^{-3}$ M and $K_{\mathrm{C8}^-,\mathrm{mic}} \approx 0.39$ M at 25 °C.[6] These values demonstrate that the transfer of the nonionic fatty acid (HC8) from the bulk into a micelle is much more favorable (about 100 times) than the transfer of the negatively-charged carboxylate ($\mathrm{C8}^-$). Additionally, from the condition for dissociation equilibrium between HC8 and $\mathrm{C8}^-$ in the bulk, we find that:

$$\frac{c_{\mathrm{C8}^-}}{c_{\mathrm{HC8}}} = \frac{K_{\mathrm{a,HC8}}}{10^{-\mathrm{pH}}}, \tag{A.7}$$

where $K_{\mathrm{a,HC8}} = 1.3 \times 10^{-5}$ M ($\mathrm{p}K_{\mathrm{a,HC8}} = 4.89$) is the acidity constant of HC8 at 25 °C.[4] Combining eq A.6 and A.7, the ratio $y_{\mathrm{C8}^-} / y_{\mathrm{HC8}}$ yields:

$$\frac{y_{\mathrm{C8}^-}}{y_{\mathrm{HC8}}} = \frac{K_{\mathrm{a,HC8}}}{10^{-\mathrm{pH}}} \frac{K_{\mathrm{HC8,mic}}}{K_{\mathrm{C8}^-,\mathrm{mic}}}. \tag{A.8}$$

Finally, the degree of HC8 ionization in the mixed micelles $\alpha$ is given by:

$$\alpha \equiv \frac{y_{\mathrm{C8}^-}}{y_{\mathrm{C8}^-} + y_{\mathrm{HC8}}} = \frac{10^{\mathrm{pH-6.91}}}{1 + 10^{\mathrm{pH-6.91}}}. \tag{A.8}$$

Figure S2a shows how the pH of the ternary micellar solution depends on the *input* HC8 concentration at fixed 70 mM CAPB and 30 mM SLES. Below 25 mM HC8, the micellar solutions are clear and their pH decreases logarithmically with the increase of HC8 concentration. At 25 mM HC8, the mixed micelles are fully-loaded with octanoic acid; hence, any excess amount of HC8 precipitates in the form of small droplets and the samples become turbid. Above 25 mM HC8, the pH levels off, because the monomer concentration $c_{\mathrm{HC8}}$ in the bulk is fixed to 4.2 mM, that is, the solubility of octanoic acid in water at 25 °C.[6]

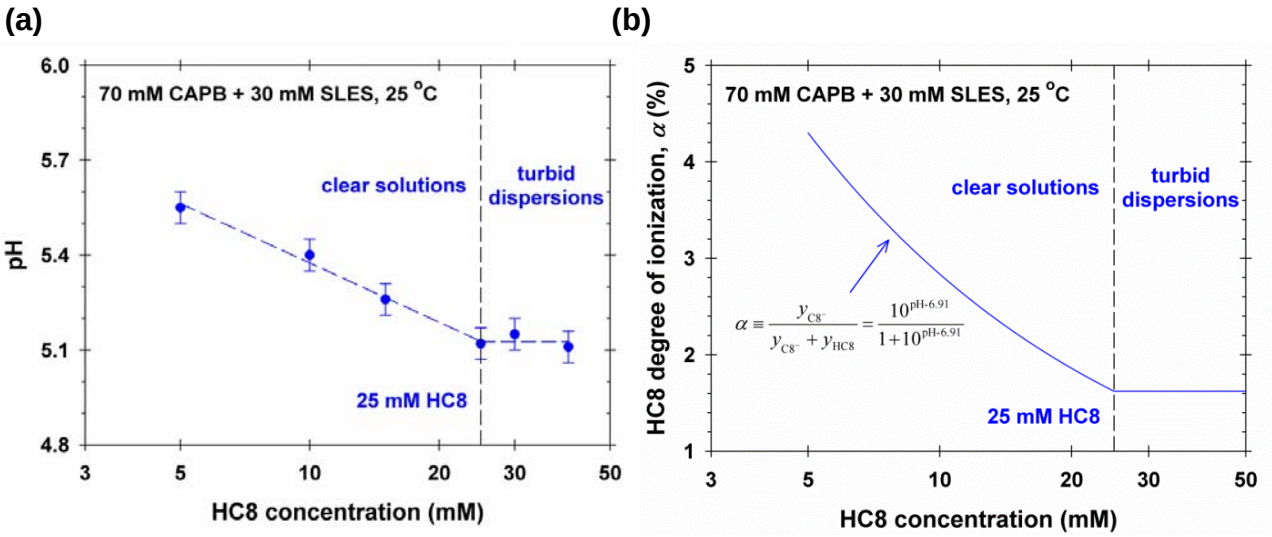


**Figure S2.** (a) The pH of the ternary mixtures is plotted versus the *input* HC8 concentration at fixed 70 mM CAPB and 30 mM SLES. The full circles represent the experimental data, whereas the dashed line follows the observed tendency. (b) Plot of $\alpha$ versus the *input* HC8 concentration at fixed 70 mM CAPB and 30 mM SLES. The solid line is calculated using eq A.8.

Using the experimental data from Fig. S2a and applying eq A.8, we calculated the degree of HC8 ionization $\alpha$ as a function of the input HC8 concentration (Fig. S2b). In Fig. S2b, $\alpha$ decreases from about 4.5 % to 1.6 % and then reaches a plateau. From these numerical results, we also see that the tri-component mixed micelles contain much more nonionic HC8 than negatively-charged $C8^-$, having $y_{HC8} / y_{C8^-} > 20$, while $C8^-$ is more abundant in the bulk, having $c_{HC8} / c_{C8^-} < 0.6$. As explained before, such partitioning in the micelles is to be expected since the nonionic HC8 more readily goes in the micelles than the negatively-charged carboxylate ($C8^-$).

### A.3. Effect of sodium octanoate (NaC8) on the micellar growth

To prove that HC8 (rather than NaC8) induces the micellar growth, we carried out additional experiments with NaC8. The samples were prepared following the experimental procedure from Section 3.2. Figure S3 shows the results of our pH and viscosity measurements of the respective NaC8-containing systems. We see that the pH increases logarithmically, whereas $\eta_0$ decreases linearly with the NaC8 concentration. The latter can be explained as follows: NaC8 increases the surface charge density of the mixed micelles; hence, they diminish in size due to increased intramicellar electrostatic repulsion between the negatively-charged headgroups and $\eta_0$ decreases (Figure S3).

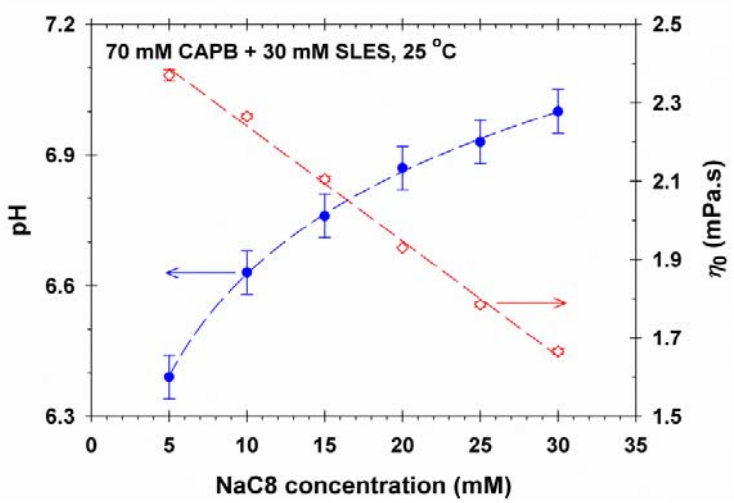


**Figure S3.** The pH and zero-shear viscosity $\eta_0$ are plotted as a function of the *input* NaC8 concentration at fixed 70 mM CAPB and 30 mM SLES. The full circles represent pH data, whereas the empty diamonds represent the measured viscosity $\eta_0$.

In contrast, the non-ionic HC8 decreases the surface charge density of the mixed micelles and serves as a spacer between the negatively-charged SLES headgroups, which leads to micellar growth; see the main text of the article.

### A.4. Additional rheological results

From Table S1, we see that around the viscosity peak the relaxation time $\tau_R$ passes through a maximum, while the elastic plateau modulus $G_0$ increases. Similar behavior was observed previously in binary (cetyltrimethylammonium bromide, CTAB, and sodium salicylate) solutions by Hoffmann & Abdel-Rahem.[7] They have shown that at the peak $\eta_0$ is controlled by reptation, whereas away from the peak $\eta_0$ is controlled by reversible scission (kinetic control).[7] The two mechanisms can be distinguished by addition of glycerol, which shortens $\tau_R$ under reptation control, but weakly affects $\tau_R$ under scission (kinetic) control.[7]

**Table S1.** Rheological properties of the studied micellar solutions around the viscosity peak at fixed total (CAPB+SLES) concentration, $c_{tot}$ = 100 mM.

| HC8 (mM) | $G_0$ (Pa) | $\tau_R$ (s) | $\eta_{\omega=0}$ (Pa·s) | $\eta_0$ (Pa·s) |
|---|---|---|---|---|
| 16 | 2.34 | 1.35 | 3.16 | 4.61 |
| 18 | 7.32 | 5.15 | 37.7 | 41.0 |
| 20 | 16.0 | 0.125 | 2.00 | 2.06 |

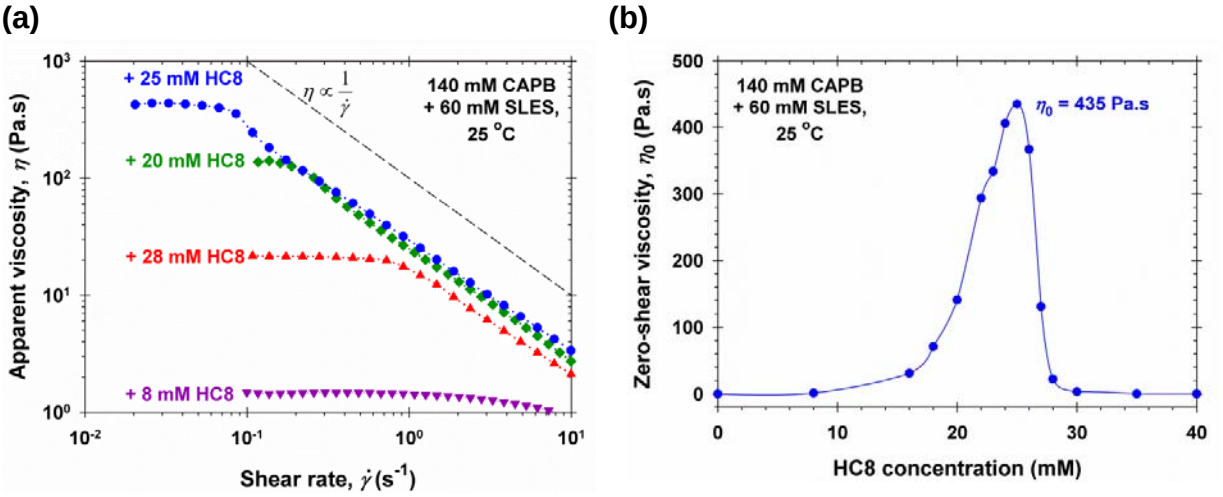


**Figure S4.** Effect of octanoic acid (HC8) on the sample's viscosity at fixed $c_{tot}$ = 200 mM (140 mM CAPB and 60 mM SLES) – data from the steady shear regime. (a) Plot of the apparent shear viscosity $\eta$ vs the shear rate $\dot{\gamma}$. (b) The zero-shear viscosity $\eta_0$ vs HC8 concentration.

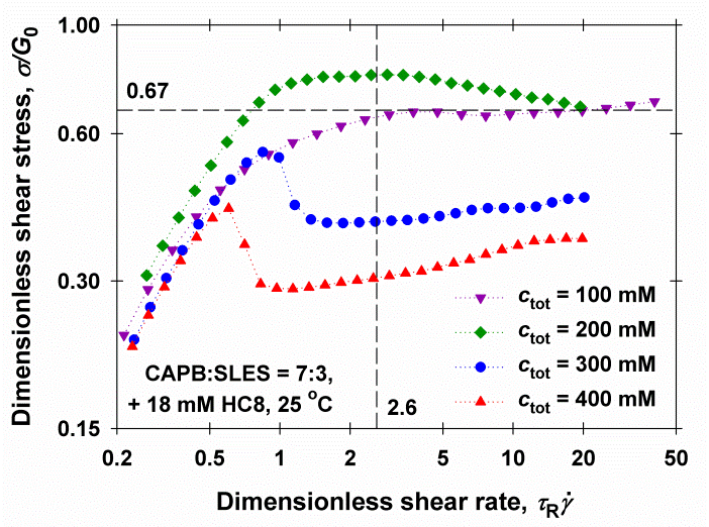


**Figure S5.** Rheological data for the ternary micellar solutions at fixed HC8 concentration of 18 mM and at four different values of the total surfactant (CAPB+SLES) concentration $c_{tot}$. The dimensionless shear stress $\sigma / G_0$ is plotted versus the dimensionless shear rate $\tau_R \dot{\gamma}$. $G_0$ and $\tau_R$ are determined from the oscillatory experiments; see Section 4.2 for details. From the curves at $c_{tot}$ = 100 and 200 mM, we see that the shear-banding plateau sets in at $\tau_R \dot{\gamma} \approx 2.6$ and the plateau value levels off at $\sigma / G_0 \approx 0.67$; see ref. 10 in the paper. However, at higher concentrations, $c_{tot}$ = 300 and 400 mM, some deviations occur, probably due to a different regime.

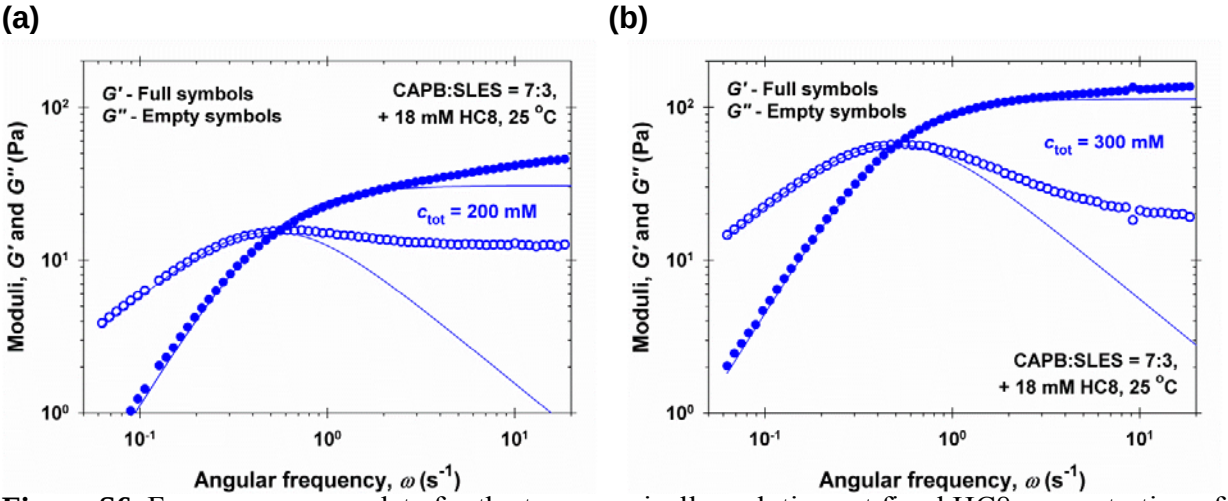


**Figure S6.** Frequency sweep data for the ternary micellar solutions at fixed HC8 concentration of 18 mM at two values of the total surfactant (CAPB+SLES) concentration, $c_{tot}$. The storage and loss moduli, $G'$ and $G''$, are plotted versus the angular frequency $\omega$. (a) $c_{tot} = 200$ mM. (b) $c_{tot} = 300$ mM. The solid lines are drawn in accordance with the pure Maxwell model.

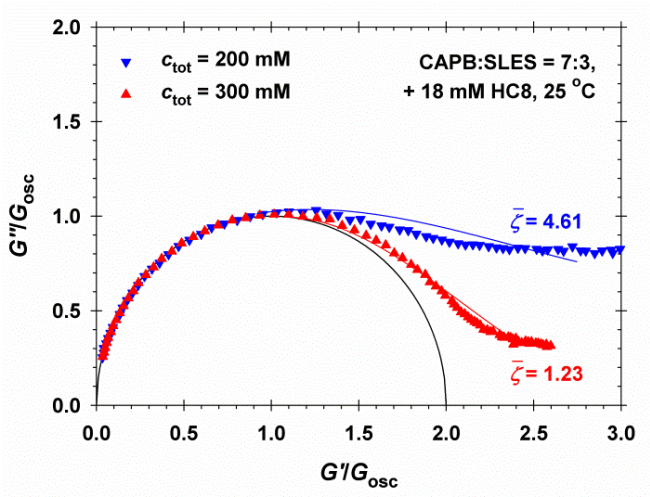


**Figure S7.** Frequency sweep data for the ternary micellar solutions at fixed HC8 concentration of 18 mM at two values of the total surfactant (CAPB+SLES) concentration, $c_{tot}$. The Cole-Cole plots depict $G''/G_{osc}$ vs $G'/G_{osc}$, where $G_{osc} = G_0/2$. The semicircle represents the pure Maxwellian behavior, whereas the solid lines represent fits of numerical data from refs. 8 and 17 in the paper.

## References

(1) *Product specification sheet of TEGO® Betain F50*, Evonik Nutrition & Care GmbH, Evonik Industries AG, Germany.

(2) Harned, H. S.; Owen, B. B. *The Physical Chemistry of Electrolytic Solutions*; 2nd ed., Reinhold Publishing Corp.: New York, 1950.

(3) Ravdel, A. A.; Ponomareva, A. M. (Eds.), *Concise Handbook of Physicochemical Quantities*; 8th ed., Khimiya: Leningrad, 1983 [in Russian].

(4) Haynes, W. M. (Ed.), *CRC Handbook of Chemistry and Physics*; 95th ed., CRC Press: Boca Raton, 2014 – 2015.

(5) Weers, J. G.; Rathman, J. F.; Axe, F. U.; Crichlow, C. A.; Foland, L. D.; Scheuing, D. R.; Wiersema, R. J.; Zielske, A. G. Effect of the Intramolecular Charge Separation Distance on the Solution Properties of Betaines and Sulfobetaines. *Langmuir* **1991**, *7*, 854–867.

(6) Tzocheva, S. S.; Kralchevsky, P. A.; Danov, K. D.; Georgieva, G. S.; Post, A. J.; Ananthapadmanabhan, K. P. Solubility limits and phase diagrams for fatty acids in anionic (SLES) and zwitterionic (CAPB) micellar surfactant solutions. *J. Colloid Interface Sci.* **2012**, *369*, 274–286.

(7) Hoffmann, H.; Abdel-Rahem, R. Influence of co-solvent on the rheological behavior of aqueous viscoelastic surfactant solutions. *Colloid Polym. Sci.* **2010**, *288* (6), 603–612.